Aeroelastic Stability Characteristics of a Composite Swept Wing with Tip Weights for an Unrestrained Vehicle

I. Lottati*
Technion—Israel Institute of Technology, Haifa, Israel

An analytical investigation to determine aeroelastic flutter and divergence behavior of a composite, forward-swept rectangular wing was conducted. It is assumed that the wing is carrying a fuselage at its semispan, a pylon at the wing tip, and that the aircraft is in a free-flight condition (unrestrained vehicle). The influence, due to the variation in the bending-torsion stiffness coupling of the tailored wing on the flutter and divergence critical dynamic pressure, is analyzed. The paper discusses the influence of the warping effect on the system's flutter and divergence velocities. The aeroelastic stability behavior of the system is obtained by applying an optimization procedure that solves exactly the coupled bending-torsion equations of motion for the unrestrained swept-wing aircraft. The results of the present study indicate that the warping effect significantly influences the system's aeroelastic characteristics.

Introduction

THE first wind-tunnel demonstration of aeroelastic tailoring of advanced composites applied to forward-swept wings (FSW)[1] showed that the orientation of a composite laminated manufactured wing could significantly affect the divergence speed of the system by introducing a bending-torsion coupling stiffness. This coupling can be used to alleviate the constraint of a lower divergence speed for the FSW vehicle without the traditional weight penalty[2] associated with it. Analytical studies and wind-tunnel testing[3] helped to demonstrate the advantages of applying aeroelastic tailoring to FSW's introduced by using composites in aircraft wing design.

The first analysis and tests performed on FSW configurations were for cantilevered wing-type models. The flutter speed of a cantilever FSW was calculated to be higher than the static divergence speed and was not considered as a particular problem of interest in FSW configurations. However, analysis[4] and tests[5] that investigated coupling of the rigid-body airplane pitch mode with the wing first bending mode, for a free-flight vehicle, predicted a dynamic instability well below the static divergence speed of the cantilevered wing. The instability has been described as pitch/bending flutter or body-freedom flutter. The coupling of the aircraft pitch mode and the wing elastic bending mode has been reported in the past by researchers investigating straight or slightly aft swept wings.[6,7] The importance of inclusion of body-freedom modes in the analysis while investigating instability of the aircraft is well known both in symmetric swept wings[8,9] and in asymmetric oblique wings[10,11] (by including the roll mode).

Since static aeroelastic divergence can be characterized as flutter at zero frequency, one should be alerted by the potential effects of inclusion of body-freedom modes upon divergence. This problem is discussed in Refs. 12–16. The importance of inclusion of the rigid body while investigating the aeroelastic divergence of antisymmetrical oblique wings was pointed out by Jones and Nisbet[17] and Weisshaar and Ashley.[18]

The present work deals with the flutter and divergence of an unrestrained FSW aircraft carrying weight (pylon) on its wing tips. It also focuses attention on the warping effect as affecting the aeroelastic stability characteristics of the system. The influence of the cross-coupling stiffness introduced by composites on the flutter and divergence velocities of the wing is also considered.

Received March 10, 1985; revision received Jan. 12, 1987.

*Senior Lecturer, Department of Aeronautical Engineering.

Aeroelastic Analysis of the Free FSW Aircraft

This analysis considers a high-aspect-ratio FSW, idealized by a box beam with a planform as shown in Fig. 1a, which derives all of its bending-torsion stiffness coupling from the laminated composite upper and lower skins. The fiber orientation relative to the spanwise reference axis is shown in Fig. 1b. The displacement assumptions are shown in Fig. 1c. Figure 1d indicates the pitch and roll of the fuselage as related to the elastic deformation of the swept wing. The uniform rectangular wing is taken as a beam-like surface carrying a fuselage at the semispan and concentrated weights at the tips. It is assumed that the resulting box beam wing structure is such that its deformation may be represented by a bending deflection $h(y)$, positive downward, along a straight reference axis (the rotation axis of Fig. 1c) and a rotation $\alpha(y)$, positive nose up, about the axis. In addition, it is further assumed that the wing chordwise sections, perpendicular to the beam's reference axis, are rigid so that the wing deformation is a function only of the spanwise coordinates, y. Hence, the deformation is assumed to be of the form

$$w(x,y) = h(y) + x_a \alpha(y) \tag{1}$$

where

$$x_a = x - ba$$

Using the box beam model, the equivalent bending and torsion stiffness EI_b and GJ, respectively, may be computed by employing the strain energy method. The strain energy U for a symmetric anisotropic laminated plate is given as[19]

$$U = \frac{1}{2}\int_0^1 \int_{-b}^{b} \left[D_{11}\left(\frac{\partial^2 w}{\partial x^2}\right)^2 + 2D_{12}\frac{\partial^2 w}{\partial x^2}\frac{\partial^2 w}{\partial y^2} + D_{22}\left(\frac{\partial^2 w}{\partial y^2}\right)^2 + 4D_{16}\frac{\partial^2 w}{\partial x^2}\frac{\partial^2 w}{\partial x \partial y} + 4D_{26}\frac{\partial^2 w}{\partial y^2}\frac{\partial^2 w}{\partial x \partial y} + 4D_{66}\left(\frac{\partial^2 w}{\partial x \partial y}\right)^2 \right] dx\,dy \tag{2}$$

where D_{ij} are the flexural moduli for N ply laminate with ply angle orientation θ and w the transverse deflection of the plate, positive downward (see Fig. 1b).

The kinetic energy is given by

$$T=\frac{1}{2}\int_0^1\int_{-b}^{b}\rho(x,y)\left(\frac{\partial w}{\partial t}\right)^2 dxdy + \frac{1}{2}\int_{b_{p_1}}^{b_{p_2}}\rho_p(x)\left(\frac{\partial w}{\partial t}\bigg|_{y=1}\right)^2 dx + \frac{1}{2}\int_{b_{f_1}}^{b_{f_2}}\rho_f(x)\left(\frac{\partial w}{\partial t}\bigg|_{y=0}\right)^2 dx \tag{3}$$

where $\rho(x,y)$ is the density of the wing, and $\rho_p(x)$ and $\rho_f(x)$ are the density of the pylon and fuselage, respectively. b_{p_1} and b_{p_2} are the forward and rearward coordinates of the pylon, respectively, while b_{f_1} and b_{f_2} represent the fuselage coordinates.

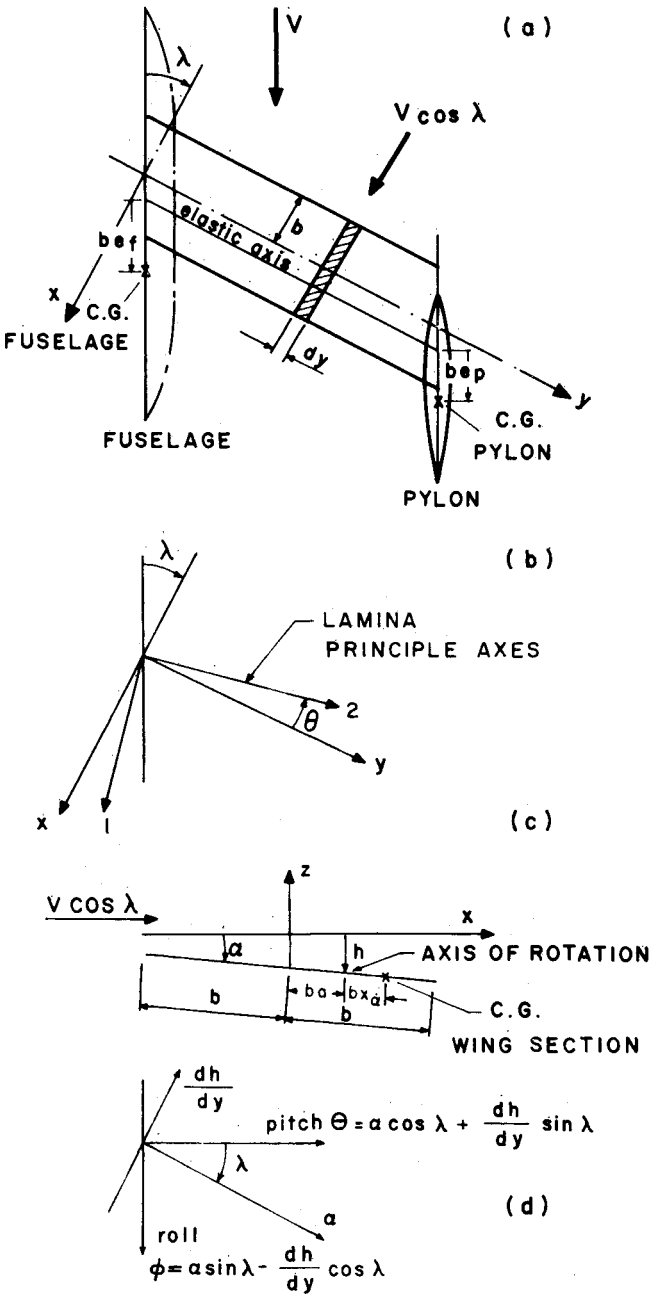

Fig. 1 Slender swept-wing planform, lamina orientation displacement assumptions, and a vector diagram of the elastic deformation and the pitch and roll of a swept wing.

The virtual work expression is given by

$$\delta W=\int_0^1(-L\delta h+M\delta\alpha)dy \tag{4}$$

where L is the aerodynamic lift, positive upward, and M the aerodynamic moment about the wing rotation axis, positive nose up. The aerodynamic forces due to the fuselage and pylon are not taken into account in the analysis.

Applying the principle of minimum potential energy, one obtains the following governing differential equations of motions:

$$EI_b\frac{\partial^4 h}{\partial y^4}+d_{22}\frac{\partial^4\alpha}{\partial y^4}+K\frac{\partial^3\alpha}{\partial y^3}+m\frac{\partial^2 h}{\partial t^2}+mX_\alpha\frac{\partial^2\alpha}{\partial t^2}=-L$$

$$d_{22}\frac{\partial^4 h}{\partial y^4}-K\frac{\partial^3 h}{\partial y^3}+S\frac{\partial^4\alpha}{\partial y^4}-GJ\frac{\partial^2\alpha}{\partial y^2}+mX_\alpha\frac{\partial^2 h}{\partial t^2}+I_\alpha\frac{\partial^2\alpha}{\partial t^2}=M \tag{5}$$

where

$m\left(=\int_{-b}^{b}\rho dx\right)$ = mass per unit span

$EI_b\left(=\int_{-b}^{b}D_{22}dx\right)$ = beam bending stiffness

$GJ\left(=4\int_{-b}^{b}D_{66}dx\right)$ = torsional stiffness

$K\left(=2\int_{-b}^{b}D_{26}dx\right)$ = bending-torsional cross-coupling stiffness. A positive K provides a wash-in elastic coupling (bend up/twist up or $-\Delta h/+\Delta\alpha$)

$S\left(=\int_{-b}^{b}D_{22}x_a^2dx\right)$ = torsional stiffness due to rigidity in tension (warping effect)

$X_\alpha\left(=\frac{1}{m}\int_{-b}^{b}\rho x_a dx\right)$ = center of mass offset from rotation axis (positive aft)

$I_\alpha\left(=\int_{-b}^{b}\rho x_a^2 dx\right)$ = section mass moment of inertia of the wing (per unit span) about its axis of rotation

$d_{22}\left(=\int_{-b}^{b}D_{22}x_a dx=-abEI_b\right)$ = coupling term due to $a\neq 0$

$d_{26}\left(=2\int_{-b}^{b}D_{26}x_a dx=-abK\right)$ = coupling terms due to $a\neq 0$

For the unrestrained aircraft, the boundary conditions are as follows:

For $y=0$ (root section),

Shear:

$$EI_b\frac{\partial^3 h}{\partial y^3}+d_{22}\frac{\partial^3\alpha}{\partial y^3}+K\frac{\partial^2\alpha}{\partial y^2}+M_f\left(\frac{\partial^2 h}{\partial t^2}+E_f\frac{\partial^2\alpha}{\partial t^2}\Big/\cos\lambda\right)=0$$

Torque and moment:

$$\cos\lambda\left(d_{22}\frac{\partial^3 h}{\partial y^3}-K\frac{\partial^2 h}{\partial y^2}+S\frac{\partial^3\alpha}{\partial y^3}-GJ\frac{\partial\alpha}{\partial y}\right)$$
$$-\sin\lambda\left(EI_b\frac{\partial^2 h}{\partial y^2}+d_{22}\frac{\partial^2\alpha}{\partial y^2}+K\frac{\partial\alpha}{\partial y}\right)$$
$$+M_f\left(E_f\frac{\partial^2 h}{\partial t^2}+K_f^2\frac{\partial^2\alpha}{\partial t^2}\Big/\cos\lambda\right)=0$$

No roll:

$$-\cos\lambda\frac{\partial h}{\partial y}+\sin\lambda\,\alpha=0$$

Warpage:

$$d_{22}\frac{\partial^2 h}{\partial y^2}+S\frac{\partial^2\alpha}{\partial y^2}+d_{26}\frac{\partial\alpha}{\partial y}=0 \tag{6}$$

where M_f is half of the mass of the fuselage, E_f the distance that the center of gravity of fuselage lies behind the wing axis of rotation and K_f the radius of gyration of the fuselage about the wing axis of rotation.

The boundary conditions at the wing tip ($y=1$) are:

Shear:

$$EI_b\frac{\partial^3 h}{\partial y^3}+d_{22}\frac{\partial^3\alpha}{\partial y^3}+K\frac{\partial^2\alpha}{\partial y^2}$$
$$-M_p\left(\frac{\partial^2 h}{\partial t^2}+E_p\cos\lambda\frac{\partial^2\alpha}{\partial t^2}+E_p\sin\lambda\frac{\partial^3 h}{\partial y\partial t^2}\right)=0$$

Torque:

$$-d_{22}\frac{\partial^3 h}{\partial y^3}+K\frac{\partial^2 h}{\partial y^2}-S\frac{\partial^3\alpha}{\partial y^3}+GJ\frac{\partial\alpha}{\partial y}$$
$$+M_p\cos\lambda\left(E_p\frac{\partial^2 h}{\partial t^2}+K_p^2\cos\lambda\frac{\partial^2\alpha}{\partial t^2}+K_p^2\sin\lambda\frac{\partial^3 h}{\partial y\partial t^2}\right)=0$$

Moment:

$$EI_b\frac{\partial^2 h}{\partial y^2}+d_{22}\frac{\partial^2\alpha}{\partial y^2}+K\frac{\partial\alpha}{\partial y}$$
$$+M_p\sin\lambda\left(E_p\frac{\partial^2 h}{\partial t^2}+K_p^2\cos\lambda\frac{\partial^2\alpha}{\partial t^2}+K_p^2\sin\lambda\frac{\partial^3 h}{\partial y\partial t^2}\right)=0$$

Warpage:

$$d_{22}\frac{\partial^2 h}{\partial y^2}+S\frac{\partial^2\alpha}{\partial y^2}+d_{26}\frac{\partial\alpha}{\partial y}=0 \tag{7}$$

where M_p is the mass of the pylon at the wing tip, E_p the distance that the center of gravity of the pylon lies behind the wing axis of rotation, and K_p the radius of gyration of the pylon about the wing axis of rotation.

It should be noted that the formulations of Goland and Luke[20] and Ruyan and Watkins[21] are indentical to the present expressions if one neglects the coupling terms d_{22} and d_{26} (which results from the fact that $a\neq 0$) for zero warpage ($S=0$) and for an unswept wing ($\lambda=0$). The aerodynamics required to solve these aeroelastic equations generally varies in levels of sophistication. Due to the complexity of the problem and in order to establish trends, the unsteady aerodynamic strip theory[22] shall be employed. The expressions for the aerodynamic forces are given in Ref. 23 as well as the expression for the approximation of the Theodorsen function $C(k)$ applied in the analysis.

The problem is solved exactly assuming an exact solution of the form

$$h/b=He^{r\eta}e^{\sigma\tau}\quad\text{and}\quad\alpha=Ae^{r\eta}e^{\sigma\tau} \tag{8}$$

where $\eta=y/1$ and $\tau=\sqrt{EI_b/ml^4}\,t$ are the nondimensional spanwise coordinate and time. Furthermore, $\sigma=\delta+i\omega$, where δ is the damping and ω the frequency of the oscillating wing (assumed real).

Incorporating the expressions for the assumed solution [Eq. (8)] in the governing equation (5) and the boundary conditions (6) and (7), one obtains the following nondimensional set of equations:

$$(r^4+\sigma^2+QL_h)H+(-ar^4+k_\alpha r^3+x_\alpha\sigma^2+QL_\alpha)A=0$$
$$(-ar^4-k_\alpha r^3+x_\alpha\sigma^2-QM_h)H$$
$$+(s_\alpha r^4-g_\theta r^2+I_\theta\sigma^2-QM_\alpha)A=0 \tag{9}$$

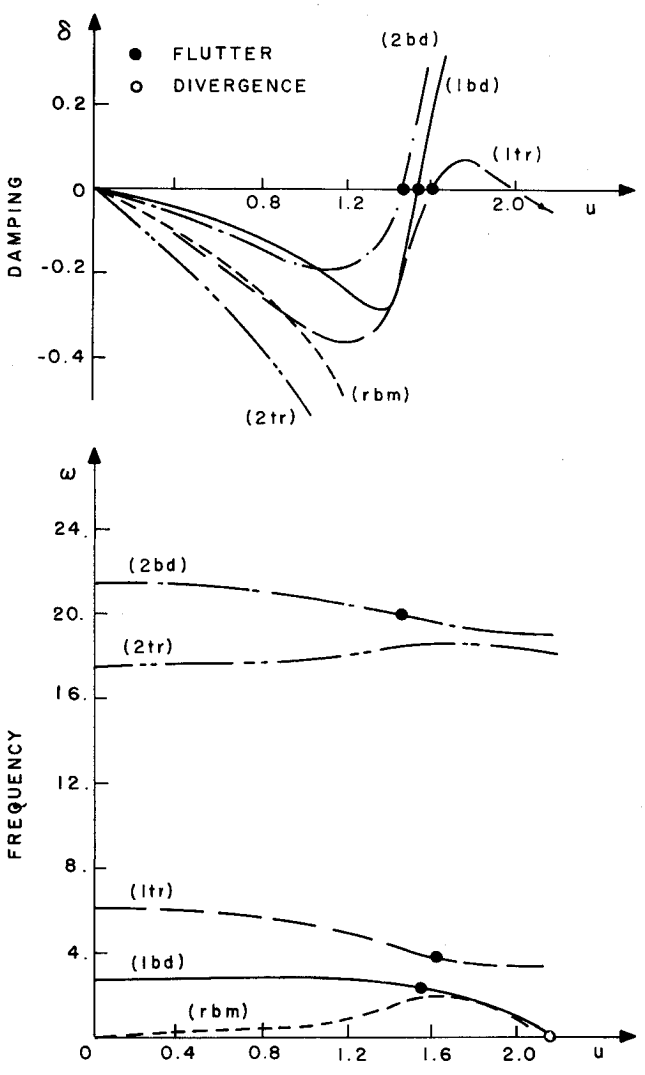

Fig. 2 Frequency and damping of the fundamental aeroelastic modes (first and second bending and torsion) and the rigid-body mode vs dimensionless airspeed (the pylon is mounted).

where

$$x_\alpha = X_\alpha/b, \quad \mathcal{R} = 1/b, \quad k_\theta = K/EI_b$$

$$k_\alpha = k_\theta \mathcal{R}, \quad s_\alpha = S/b^2 EI_b, \quad g_g = GJ/EI_b$$

$$g_\theta = g_g(\mathcal{R})^2, \quad I_\theta = I_\alpha/mb^2, \quad Q = \pi\rho v^2 l^4/EI_b$$

where L_h, L_α, M_h, and M_α are the aerodynamic coefficients (given in Ref. 23).

The boundary conditions are:

For $\eta = 0$ (root section),

$$r^3 H + (-ar^3 + k_\alpha r^2)A + m_f\sigma^2(H + e_f A/\cos\lambda) = 0$$

$$\cos\lambda[(-ar^3 - k_\alpha r^2)H + (s_\alpha r^3 - g_\theta r)A]$$
$$+ \mathcal{R}\sin\lambda[-r^2 H + (ar^2 - k_\alpha r)A]$$
$$+ m_f\sigma^2(e_f H + k_f^2 A/\cos\lambda) = 0$$

$$-r\cos\lambda H + \mathcal{R}\sin\lambda A = 0$$

$$-ar^2 H + (s_\alpha r^2 - ak_\alpha r)A = 0 \qquad (10)$$

where $m_f = M_f/ml$, $e_f = E_f/b$, and $k_f = K_f/b$.

For $\eta = 1$ (wing tip),

$$\{r^3 H + (-ar^3 + k_\alpha r^2)A$$
$$- m_p\sigma^2[(1 + e_p r\sin\lambda/\mathcal{R})H + e_p\cos\lambda A]\}e^r = 0$$

$$\{(-ar^3 - k_\alpha r^2)H + (s_\alpha r^3 - g_\theta r)A$$
$$- m_p\cos\lambda\sigma^2[(e_p + k_p^2 r\sin\lambda/\mathcal{R})H + k_p^2\cos\lambda A]\}e^r = 0$$

$$\{r^2 H + (-ar^2 + k_\alpha r)A + m_p(\sin\lambda/\mathcal{R})\sigma^2[(e_p$$
$$+ k_p^2 r\sin\lambda/\mathcal{R})H + k_p^2\cos\lambda A]\}e^r = 0$$

$$[-ar^2 H + (s_\alpha r^2 - ak_\alpha r)A]e^r = 0 \qquad (11)$$

where $m_p = M_p/ml$, $e_p = E_p/b$, and $k_p = K_p/b$.

To obtain a nontrivial solution, the determinant of the system of equations (9) has to be zero [$\Delta(r,\sigma) = 0$ forming the characteristic polynomials in r and σ of the problem]. For prescribed σ, the zero determinant condition [$\Delta(r,\sigma) = 0$] has to be applied to obtain the root r_i of the characteristic polynomials of the system. The roots r_i with the prescribed σ must satisfy the boundary conditions given by Eqs. (10) and (11). Thus, to satisfy the boundary conditions, the determinant of the set of linear equations [(10) and (11)] has to be equal to zero [$\Delta_b(r,\sigma) = 0$] to reach a nontrivial solution.

The combination of ω and Q (minmum) fulfilling the conditions $\Delta(r,\sigma) = 0$ and $\Delta_b(r,\sigma) = 0$, which will bring the system from neutral stability ($\delta = 0$) to instability ($\delta > 0$), are the conditions at which the wing will undergo dynamic ($\omega \neq 0$) or static ($\omega = 0$) instability. It should be noted that whenever the warpage effect is neglected, the degree of the characteristic polynomials $\Delta(r,\sigma) = 0$ is reduced from the eighth to the sixth degree and, thus, the two boundary conditions associated with the warpage effect must be omitted. The numerical procedure of the solution is outlined in the appendix of Ref. 23.

As mentioned, the static aeroelastic divergence formulation can be obtained from the dynamic expressions by assuming zero frequency ($\omega = 0$ and, thus, $\sigma = \delta$).

Applications

In order to verify the accuracy of the flutter analysis, a comparison study was conducted with the numerical example given by Goland and Luke.[20] This example consists of an aircraft having a rigid fuselage and carrying a pylon in its wing tips in a symmetric free flight (unrestrained vehicle). The vehicle has a uniform rectangular unswept wing ($\mathcal{R} = 6.16$) of constant mass per unit span with the following properties:

$m = 149.5$ lb	$l = 19.4$ ft
$EI_b = 18.09 \times 10^6$ lb·ft^2	$x_\alpha = 0.16$
$GJ = 4.68 \times 10^6$ lb·ft^2	$a = -0.36$
$\rho = 2.3769 \times 10^{-3}$ slug/ft^3	$e_f = -0.455$
$m_f = 1.2757$	$e_p = 0$
$m_p = 0.3641$	$k_f = 2.2759$
$b = 3.15$ ft	$k_p = 0.6603$ (12)

To test the efficiency and accuracy of the present numerical method and for the sake of comparison, the classical bending-torsion formulation[20] is considered first (hence $d_{22} = d_{26} = S = 0$).

Figure 2 presents the variation of the frequencies and damping of the first and second bending and torsion modes vs the nondimensional velocity of the flow ($u = v/v_{\text{ref}}$, where $v_{\text{ref}} = 400$ mph). Figure 2 illustrates how the frequency of the first bending mode (1bd) drops while increasing the velocity u until it interacts with the rigid-body mode (rbm) and flutters at $u_{\text{cr}} = 1.556$. The frequency of the first torsion mode (1tr) also drops, while increasing the velocity u interacts with the first bending mode and flutters at $u_{\text{cr}} = 1.620$. Figure 2 shows that the second bending mode (2bd) interacts with the second torsion mode (2tr) and flutters at an even lower speed than the first bending and torsion modes ($u_{\text{cr}} = 1.474$). Goland and Luke[20] overlooked the fact that the first and second bending modes encountered flutter; in their calculation, the only mode that fluttered was the first torsion mode. Housner and Stein[24] worked out the same example and found out that the first and second bending modes did indeed undergo flutter instability; their results are in very good agreement with the results obtained herein (see Table 1). The small differences between the results of the different method, as given in Table 1, are probably due to the different types of approximation for Theodorsen's circulation function applied in the analysis. Recall that the results displayed in Fig. 2 are accurate at the flutter condition ($\delta = 0$) only, due to the fact that the air forces have not been introduced in a sufficiently general form to account for possible convergent or divergent oscillations. It should be further noted that the curves in Fig. 2 are labeled according to their origin at zero airspeed. As depicted in Fig. 2, the frequency of the first bending mode drops while the frequency of the rigid-body mode increases as the velocity of the flow increases, causing the elastic first bending mode to flutter. The frequency of the first bending mode continues to drop (post flutter) as the velocity increases until it becomes zero and diverges. Studies[4,5,26] on FSW's in free flight reveal behavior similar to that depicted in Fig. 2, indicating that the first bending mode coalesces with the short-period mode, causing rigid-body pitch/wing bending flutter or body-freedom flutter to occur. As stated, the aerodynamic forces on the fuselage and pylon are not taken into account, thus the rigid pitch mode plotted in Fig. 2 is due to the aerodynamic forces on the wing only. Nevertheless, the fuselage and pylon influence the stability behavior of the system through the boundary conditions at the root and wing tips. It should be noted that, for a static unstable aircraft ($e_f > 0$ for the unswept wing), the rigid pitch mode will diverge ($\omega = 0$, $\delta > 0$).

Figure 3 illustrates the variation of the flutter instability of the three critical modes vs the distance of the center of gravity of the pylon from the wing axis of rotation (e_p). Figure 3

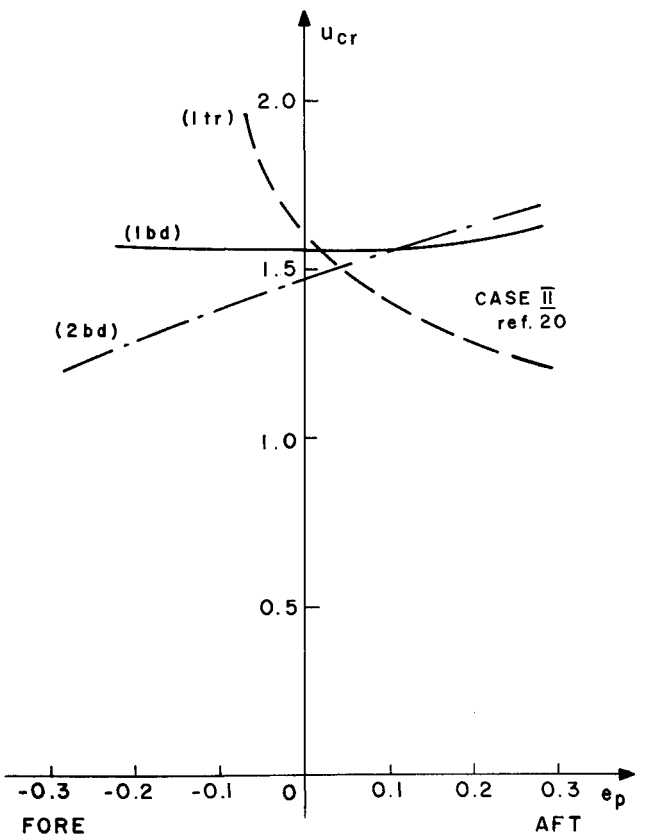

Fig. 3 Variation of the flutter velocity of the system due to changes of the distance that the center of gravity of the pylon lies behind the wing axis of rotation (e_p).

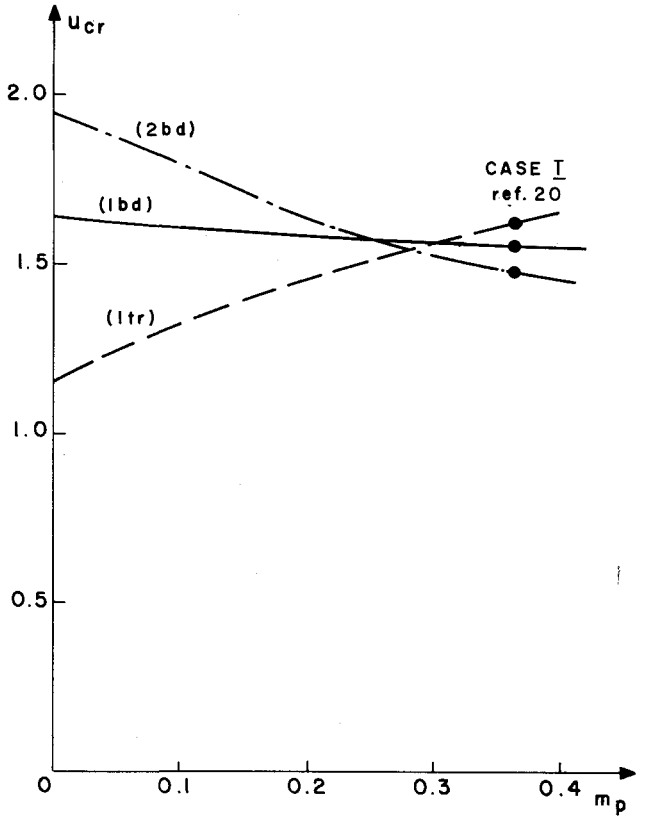

Fig. 4 Variation of the flutter velocity of the system due to variation of the mass of the attached pylon (m_p).

Table 1 Flutter speed comparison for the Goland & Luke[20] example of a uniform rectangular unswept wing with attached fuselage and tip weights in free-flight condition

Method of computaton	Description	Flutter speed,[a] u	Flutter frequency,[b] ω	Mode of instability
Present	Exact	1.620	3.701	1tr
Goland & Luke[20]	Exact	1.637	3.654	1tr
COMBOF,[24]	31 Finite-difference stations	1.630	3.654	1tr
SADSAM,[c 25]	10 Finite elements	1.630	3.703	1tr
Present	Exact	1.556	2.171	1bd
COMBOF	31 Finite-difference stations	1.544	2.168	1bd
SADSAM	10 Finite elements	1.538	2.168	1bd
Present	Exact	1.474	19.774	2bd
COMBOF	31 Finite-difference stations	1.465	19.743	2bd
SADSAM	10 Finite element	1.493	19.408	2bd

[a] u is normalized by $v_{ref} = 400$ mph. [b] ω is normalized by $\omega_{ref} = 0.835$ Hz. [c] Reproduced from Ref. 24.

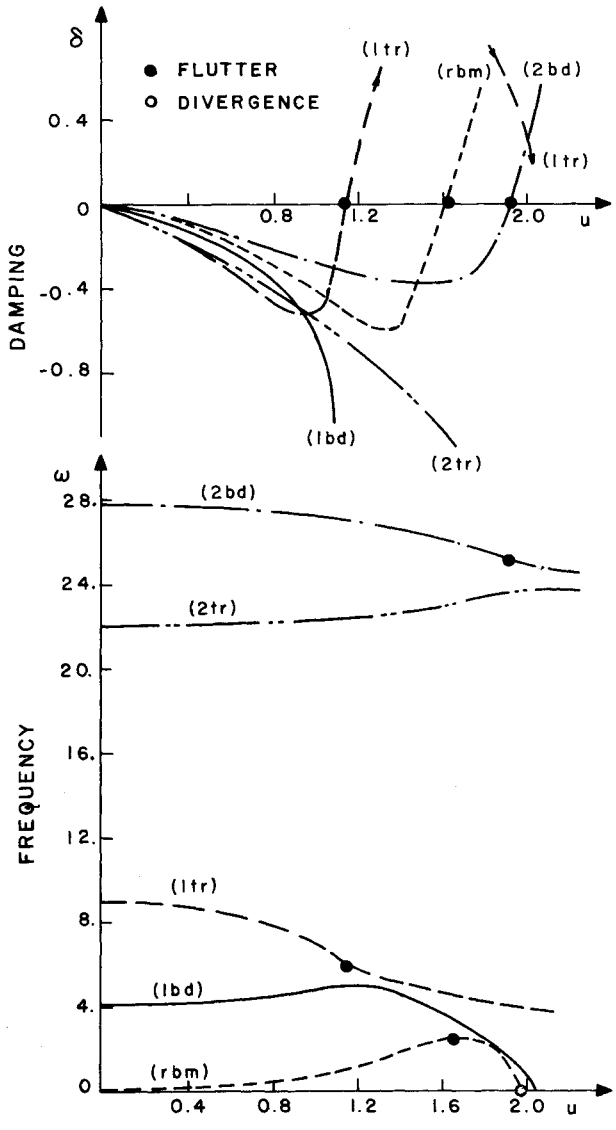

Fig. 5 Frequency and damping of the fundamental modes vs airspeed for the system without the pylon ($m_p = 0$).

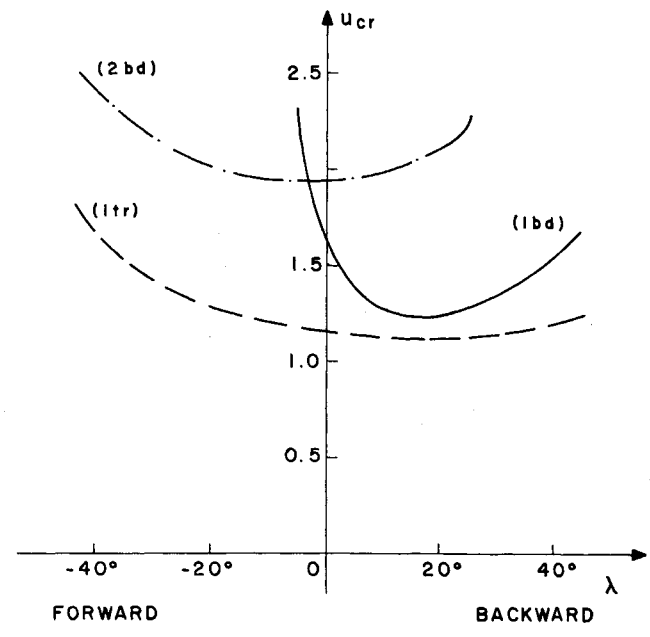

Fig. 6 Variation of the flutter velocity due to changes in sweep angle of the wing for the system without the pylon ($m_p = 0$).

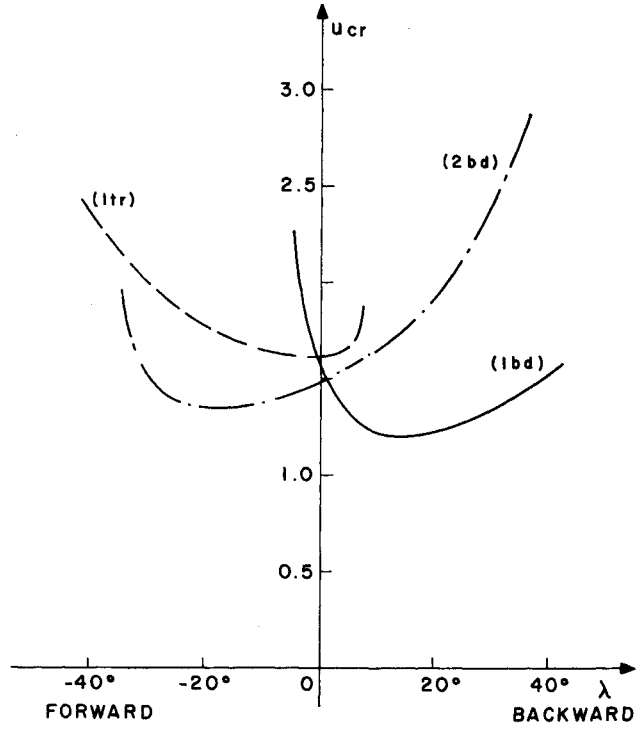

Fig. 7 Variation of the flutter velocity due to changes in sweep angle of the wing for the system while the pylon is mounted.

shows that, as the location of the center of gravity of the pylon is moved aft ($e_p > 0$), the flutter of the first torsion mode drops significantly (case II of Ref. 20 is indicated for the sake of comparison). Moving the center of gravity of the tip weights forward ($e_p < 0$) causes the flutter of the second bending mode to drop significantly. The results of Fig. 3 indicate that a slight move of the pylon backwards will be beneficial.

Figure 4 depicts the variation of the flutter velocity of the critical modes vs the variation of the weight of the pylon at the tip. The results plotted in Fig. 4 indicate that the flutter speed of the first torsion mode increases as the pylon's weight increases, while the flutter speed of the second bending mode shows an opposite trend of behavior (the two curves intersect at about $m_p \sim 0.3$).

Figure 5 shows the variation of the frequencies and damping of the first and second elastic modes, including the rigid-body mode, for the system without the pylon attached at the tips ($m_p = 0$). The results of Fig. 5 show that the first bending mode interacts with the first torsion mode, causing the first torsion mode to flutter and then at a higher velocity, the first bending mode interacts with the rigid-body mode causing it to flutter (labeled 1bd mode in Fig. 4). It should be noted that the flutter of the rigid-body mode changed to divergence instability at a higher velocity (post flutter). The second bending mode also encountered flutter, but at a higher velocity than the flutter of the first torsion and rigid-body modes.

Figures 6 and 7 show the variation of the critical flutter velocity vs the sweep angle of the wing for the cases in which the pylon is not or is mounted at the wing tips, respectively. The results of Fig. 6 indicate that the flutter of the first torsion mode is the lowest for all ranges of sweep angles (the $m_p = 0$ case). The results of Fig. 7 (pylon mounted) indicate that the flutter velocity of the first bending mode drops significantly for backward sweep angles (reaching a minimum around 15 deg sweep), while the flutter of the sec-

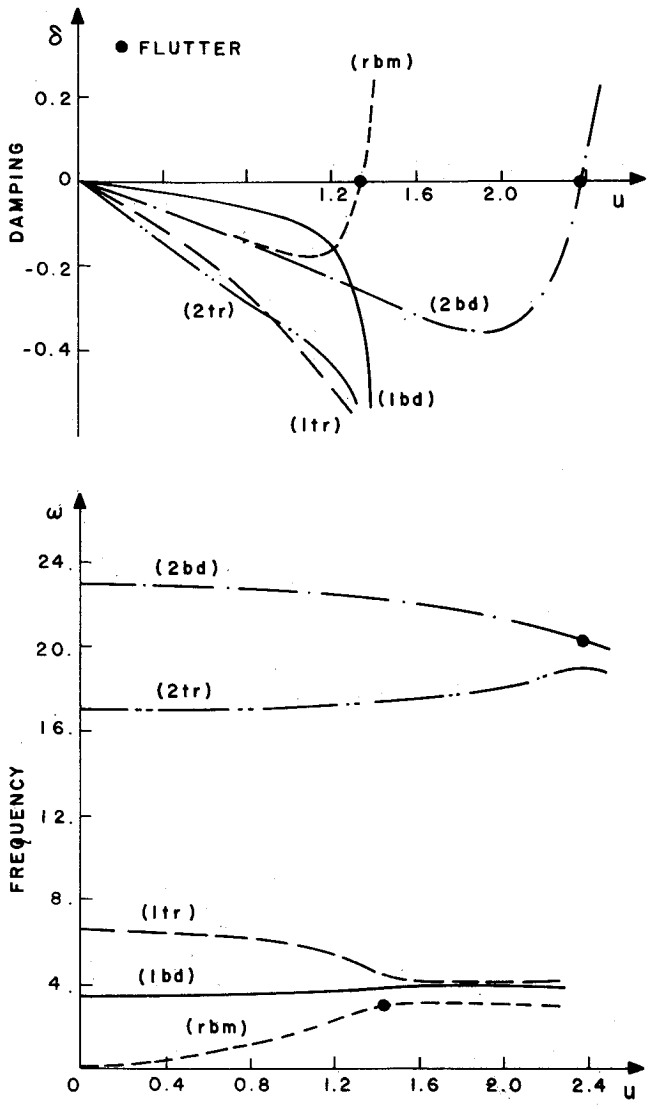

Fig. 8 Frequency and damping of the fundamental modes vs airspeed for a backward-swept wing ($\lambda = 30$ deg) while the pylon is mounted.

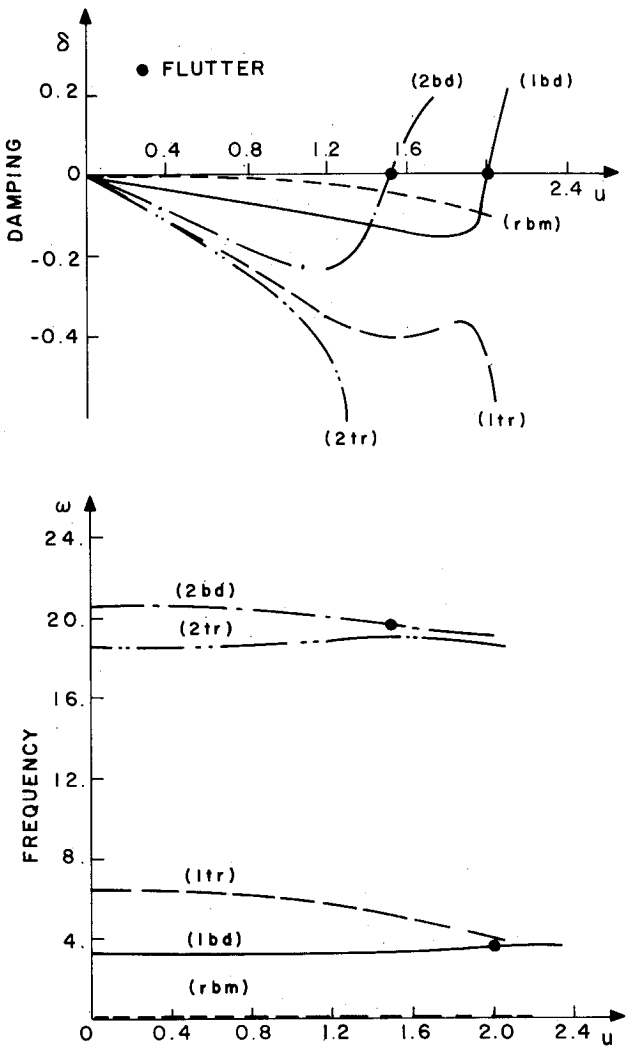

Fig. 9 Frequency and damping of the fundamental modes vs airspeed for a forward-swept wing ($\lambda = -30$ deg) while the pylon is mounted.

ond bending mode drops appreciably for a forward sweep angle (reaching a minimum around -20 deg sweep).

Figures 8 and 9 show the variation of aeroelastic behavior of the elastic and rigid-body modes vs the flow velocity for a backward-/forward-swept wing at a sweep angle of $|\lambda| = 30$ deg, respectively, while the pylon is mounted at the tips. The results of Fig. 8 ($\lambda = 30$ deg) indicate that the rigid-body mode undergoes flutter (labeled 1bd in Fig. 7) and the second bending mode encounters flutter at a higher velocity. It should be noted that, even though the first bending and first torsion modes coalesce, neither of them undergo flutter.[27]

The results of Fig. 9 ($\lambda = -30$ deg) indicate that the first bending mode interacts with the first torsion mode and encounters flutter, but the second bending mode undergoes flutter at a lower velocity as compared to the first bending mode. It should be noted that the aeroelastic behavior of the rigid-body mode, as shown in Fig. 9, indicates that it has very low damping and frequency, indicating that the rigid-body mode may be unstable if the wing is swept further forward (the vehicle may become statically unstable). The influence of the coupling terms d_{22} and d_{26} and the warpage effect is subsequently addressed.

As can be seen from the characteristic equation (9), the coupling terms d_{22} and d_{26} and the parameter s_α can significantly affect the stability behavior of the system. The inclusion of these parameters increases the degree of the characteristic equation from the sixth to the eighth power. Furthermore, these parameters affect the boundary conditions of the problem and, thus, potentially might influence the results.

Figure 10 presents the variation of the frequencies and damping of the elastic and rigid-body modes vs the velocity u, taking into account the warping effect $s_\alpha = 1/3 + a^2$ (with the pylon mounted at the tips). The main effect of including the s_α term results in an increase of the frequency of the second bending mode (compare Figs. 2 and 10), and it alters the aeroelastic behavior of this mode to undergo flutter instability at higher velocity as compared to the $s\alpha = 0$ case. The inclusion of the s_α term did not change the stability behavior of the rigid-body mode and the first bending and first torsion elastic modes.

Figure 11 shows the variation of flutter velocity vs the sweep angle of the wing, taking into account the s_α terms. For the sake of comparison, the results of Fig. 7 are reproduced in Fig. 11. The comparison depicted in Fig. 11 reveals that the first torsion and first bending modes are not influenced by the inclusion of the warpage, while the second bending mode is significantly influenced by it. The results of Fig. 11 also indicate that by sweeping the wing forward one can significantly raise the flutter velocity of the wing (the vehicle has to be statically stable).

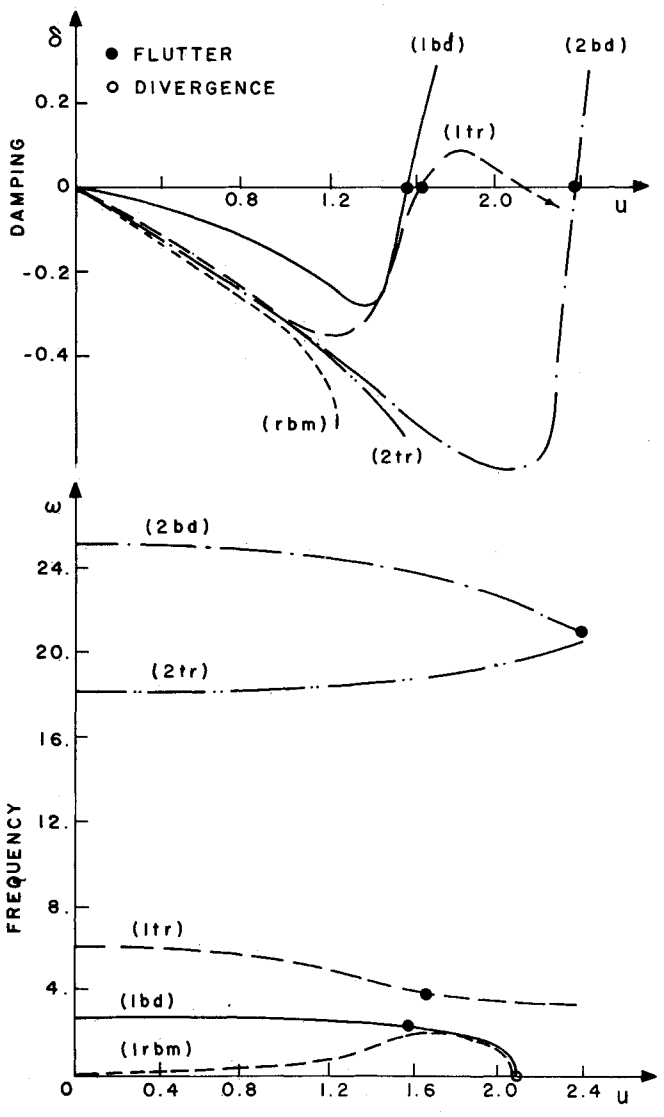

Fig. 10 Frequency and damping of the fundamental modes vs airspeed for an unswept wing while including the warping term in the analysis (the pylon is mounted).

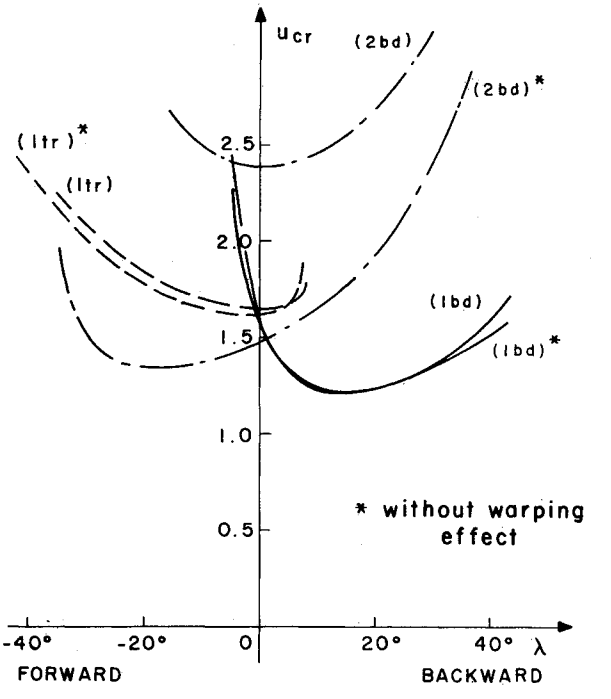

Fig. 11 Comparative study of the variation of the flutter velocity of the system due to changes in sweep angle of the wing with and without the inclusion of the warping effect (the pylon is mounted).

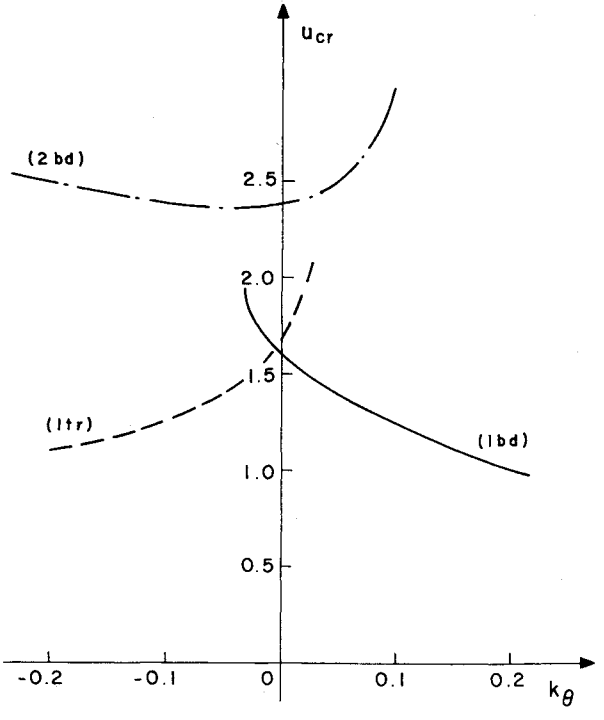

Fig. 12 Variation of the flutter velocity of the system due to changes in the cross-coupling stiffness coefficient (k_θ) while including the warping term (the pylon is mounted).

Figure 12 shows the variation of the system's flutter velocity vs the cross-coupling stiffness k_θ introduced by the composites while including the s_α terms. The results of Fig. 12 indicate that the flutter of the first bending mode drops significantly for a postitive cross coupling (bend up/twist nose up), while the flutter of the first torsion mode drops significantly for a negative cross-coupling stiffness. Thus, if the wing is to be swept forward, a positive cross coupling will be preferable to alleviate significantly the flutter instability of the system.

Figure 13 presents the variation of the frequencies and damping of the elastic and rigid-body modes vs the velocity u taking into account d_{22} and d_{26} while including the warping (with the pylon mounted at the tips). The main effect of including the coupling terms d_{22} and d_{26} is that the first torsion mode flutters at a lower velocity as compared to the $d_{22}=d_{26}=0$ case (Fig. 10) and the first bending mode does not undergo instability. The results of Fig. 13 indicate that although the rigid-body mode coalesces with the first bending and first torsion modes, it does not undergo flutter instability.[27]

Figure 14 shows the variation of flutter velocity vs the sweep angle of the wing for various values of cross-coupling stiffness, taking into account the d_{22} and d_{26} coupling terms including warping. The results of Fig. 14 reveal that introducing positive cross coupling may alleviate significantly the flutter of the forward- or backward-swept wing (the first bending mode does not flutter for $k_\theta=0.1$). The divergence instability of the system is considered subsequently.

As stated, the divergence is defined as static instability ($\omega=0$, $\delta>0$) and may be computed from the dynamic formulation by letting the frequency be zero. First, we will deal with the simplest case, namely, an unswept wing with zero

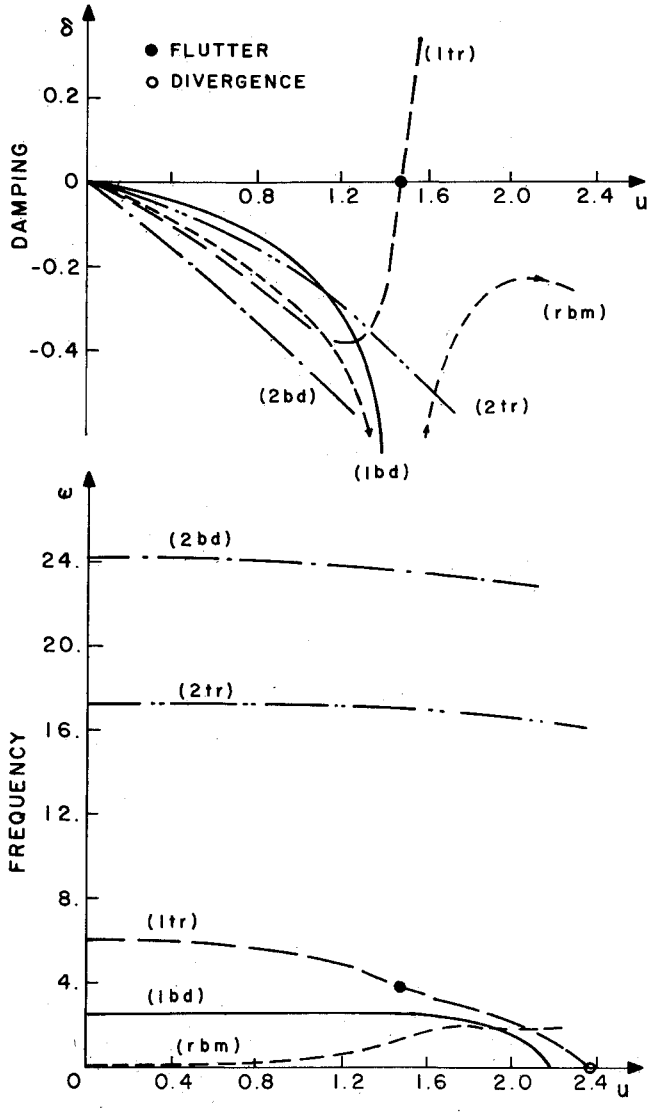

Fig. 13 Frequency and damping of the fundamental modes vs airspeed for an unswept wing while including d_{22}, d_{26}, and the warping term in the analysis (the pylon is mounted).

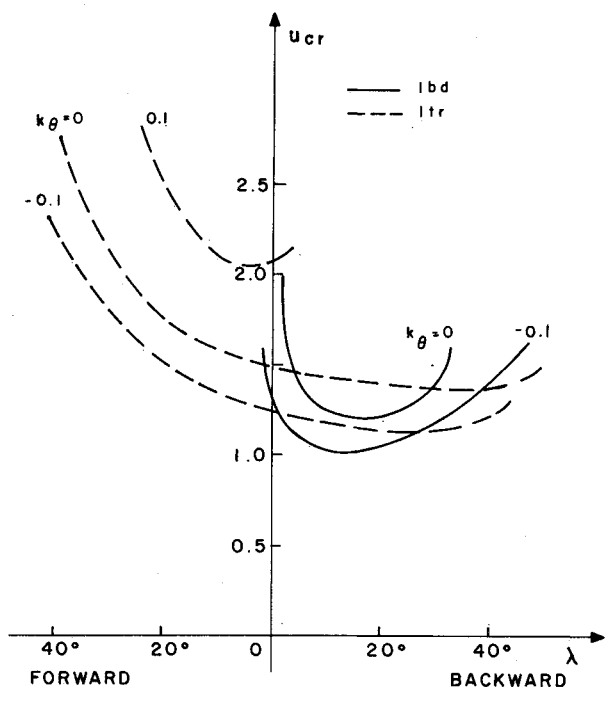

Fig. 14 Variation of the flutter velocity of the system due to changes in the sweep angle of the wing for various values of the cross-coupling stiffness coefficient (k_θ) while including d_{22}, d_{26}, and the warping term in the analysis (the pylon is mounted).

cross coupling, while $d_{22}=d_{26}=s_\alpha=0$. For this case, assuming the system to be on the onset of divergence and, thus, the governing equation associated with the torsion mode reads [Eq. (9)]

$$-g_\theta \frac{\partial^2 \alpha}{\partial y^2} - 2Qa_2\alpha = 0 \tag{13}$$

where $a_2 = \frac{1}{2} + a$ (equivalent to e, the distance between wing quarter-chord and the rotation axis) and the boundary conditions are [Eqs. (10) and (11)]

$$\frac{\partial \alpha}{\partial \eta} \text{ at } \eta = 0 \text{ and } \eta = 1 \tag{14}$$

Investigating the instability of the preceding problem reveals that the system does not have a distinct divergence mode (infinite dynamic pressure) as compared to the cantilevered wing type. This fact means that the only way that an unrestrained aircraft may diverge is in a post-flutter situation. Indeed, Figs. 2 and 10 show that the first bending mode undergoes divergence, Fig. 5 shows that the rigid-body mode undergoes divergence, and Fig. 13 shows that the first torsion mode undergoes divergence always in a post-flutter situation. It should be noted that the divergence characteristics of a very stable aircraft (i.e., tailed vehicle), with a fundamental bending frequency exceeding the first torsion frequency, may be different from the configuration tested in the present work.

Concluding Remarks

Despite the limitations imposed upon the study by the model's restriction assumptions, the model contains essential features to study the stability of an unrestrained vehicle. Some interesting aspects of the influence of the weight of the pylon attached at the wing tips are studied while incorporating the boundary conditions of unrestrained aircraft in the analysis. The study indicates that the warping effect and coupling terms have a significant influence on the dynamic behavior of the system. Furthermore, it is shown that the aeroelastic tailoring of the wing can alleviate appreciably the flutter instability of the forward-swept wing configuration. Unlike the cantilevered wing-type configuration, the flutter instability of the unrestrained vehicle is more critical than the divergence mode of instability.

References

[1]Sherrer, V. C., Hertz, T. J., and Shirk, M. H., "Wind Tunnel Demonstration of the Principle of Aeroelastic Tailoring Applied to Forward Swept Wings," AIAA Paper 80-0796, May 1982.

[2]Krone, N. J., "Divergence Elimination with Advanced Composite," AIAA Paper 75-1009, Aug. 1975.

[3]Hertz, T. J., Shirk, M. H., Ricketts, R. H., and Weisshaar, T. A., "On the Track of Practical Forward Swept Wings," *Astronautics & Aeronautics*, Vol. 20, Jan. 1982, pp. 40-52.

[4]Miller, G. D., Wykes, J. H., and Brosnan, M. J., "Rigid Body-Structural Mode Coupling on a Forward Swept Wing Aircraft," *Journal of Aircraft*, Vol. 20, Aug. 1983, pp. 696-702.

[5]Weisshaar, T. A., Zeiler, T. A., Hertz, T. J., and Shirk, M. H., "Flutter of Forward Swept Wings, Analysis and Tests," AIAA Paper 82-0646, May 1982.

[6]Gaukroger, D. R., "Wind Tunnel Flutter Tests on Model Delta Wings Under Fixed and Free-Root Conditions," British ARC, R&M 2826, 1955.

[7]Cunningham, H. J. and Lundstrom, R. R., "Description and

Analysis of a Rocket-Vehicle Experiment on Flutter Involving Wing Deformation and Body-Motions," NACA TN-3311, Jan. 1955.

[8]Frazer, R. A. and Duncan, W. J., "Wing Flutter as Influenced by the Mobility of the Fuselage," British ARC, R&M 1207, 1929.

[9]Gaukroger, D. R., "Wing Flutter," *AGARD Manual on Aeroelasticity*, Pt. V, 1960, Chap. 2.

[10]Weisshaar, T. A. and Crittenden, J. B., "Flutter of Asymmetrically Swept Wings," *AIAA Journal*, Vol. 14, Aug. 1976, pp. 993-994.

[11]Crittenden, J. B., Wiesshaar, T. A., Johnson, E. H., and Rutkowski, M. A., "Aeroelastic Stability Characteristics of the Oblique Winged Aircraft," *Journal of Aircraft*, Vol. 15, July 1978, pp. 429-434.

[12]Hancock, G. J., "The Static Aeroelatic Deformation of Slender Configuration, Part III: Static Stability," *The Aeronautical Quarterly*, Vol. XIV, Feb. 1963, pp. 75-104.

[13]Rodden, W. P., "Aeroelastic Divergence of Unrestrained Vehicles," *Journal of Aircraft*, Vol. 18, Dec. 1981, pp. 1072-1073.

[14]Rodden, W. P., "Aeroelastic Divergence of Unrestrained Vehicles," *Journal of Aircraft*, Vol. 21, Jan. 1984, pp. 94-96.

[15]Rodden, W. P. and Bellinger, E. D., "Aerodynamic Lag Functions, Divergence and the British Flutter Method," *Journal of Aircraft*, Vol. 19, July 1982, pp. 596-598.

[16]Rodden, W. P. and Bellinger, E. D., "Unrestrained Aeroelastic Divergence in a Dynamic Stability Analysis," *Journal of Aircraft*, Vol. 19, Sept. 1982, pp. 796-797.

[17]Jones, R. T. and Nisbet, J. W., "Aeroelastic Stability and Control of the Oblique Wing," *The Aeronautical Journal of the Royal Aeronautical Society*, Vol. 80, Aug. 1976, pp. 365-369.

[18]Weisshaar, T. A. and Ashley, H., "Static Aeroelasticity and the Flying Wing, Revisited," *Journal of Aircraft*, Vol. 11, Nov. 1974, pp. 718-728.

[19]Ashton, J. E. and Whitney, J. M., *Theory of Laminated Plates*, Technonic Publishing, Stamford, CT, 1970.

[20]Goland, M. and Luke, Y. L., "The Flutter of a Uniform Wing with Tip Weights," *Journal of Applied Mechanics*, Vol. 15, No. 1, March 1948, pp. 13-20.

[21]Runyan, H. L. and Watkins, C. E., "Flutter of a Uniform Wing with an Arbitrarily Placed Mass According to a Differential Equation Analysis and a Comparison with Experiments," NACA Rept. 966, Nov. 1948.

[22]Bisplinghoff, R. L., Ashley, H., and Halfman, R. L., *Aeroelasticity*, Addison-Wesley, Reading, MA, 1955, Chap. 7.

[23]Lottati, I., "Flutter and Divergence Aeroelastic Characteristics for Composite Forward Cantilevered Wing," *Journal of Aircraft*, Vol. 22, Nov. 1985, pp. 1001-1007.

[24]Housner, J. M. and Stein, M., "Flutter Analysis of Swept-Wing Subsonic Aircraft with Parameter Studies of Composite Wings," NASA TN-D-7539, Sept. 1974.

[25]Peterson, L., *SADSAM User's Manual*, MSR-10, MacNeal-Schwendler Corp., Dec. 1970.

[26]Noll, T. E., Eastep, F. E., and Calico, R. A., "Active Suppression of Aeroelastic Instabilities on a Forward Swept Wing," AIAA Paper 83-0991, May 1983.

[27]Nissim, E. and Lottati, I., "An Optimization Method for the Determination of the Important Flutter Modes," *Journal of Aircraft*, Vol. 18, Aug. 1981, pp. 663-668.